Title

Prediction of Metastable States for Throttling in Pressure Relief Valves for Sustainable CO_2 Heat Pump Technologies

Journal

ASME JOURNAL OF HEAT AND MASS TRANSFER, 148(6)

ISSN

2832-8450

Authors

Hughley, Jasmine

Carey, Van P

Schutzius, Thomas

Publication Date

2026-06-01

DOI

10.1115/1.4071445

ASME Journal of Heat and Mass Transfer
Online journal at:
https://asmedigitalcollection.asme.org/heattransfer

Prediction of Metastable States for Throttling in Pressure Relief Valves for Sustainable CO_2 Heat Pump Technologies

Jasmine Hughley[1]
Mem. ASME
Energy and Multiphase Transport Laboratory,
Department of Mechanical Engineering,
University of California-Berkeley,
Berkeley, CA 94720
e-mail: Jasmine_hughley@berkeley.edu

Van P. Carey
Mem. ASME
Energy and Multiphase Transport Laboratory,
Department of Mechanical Engineering,
University of California-Berkeley,
Berkeley, CA 94720
e-mail: vpcarey@berkeley.edu

Thomas Schutzius
Mem. ASME
Department of Mechanical Engineering,
University of California-Berkeley,
Berkeley, CA 94720
e-mail: tschutzius@berkeley.edu

Incorporating carbon dioxide (CO_2) refrigerant into the heat pump (HP) technology can reduce climate change effects due to working fluid loss. However, CO_2 refrigerants in an HP system may change from a gaseous state to a liquid or solid "snow" during the throttling and pressure-relief valve processes, which may block downstream flow in pipes and cause unsafe operation issues. This paper describes a Soave–Redlich–Kwong (SRK) statistical-thermodynamics-based model to predict CO_2 refrigerant metastable state properties (enthalpy, temperature, and volume) exhibited during throttling through a leakage path or pressure relief valve in HP technologies. In addition, the simulation can predict changes in density fluctuations states exhibited during the process that can indicate an impending phase change and can predict exit state conditions for widely varying supercritical initial equilibrium states. Results indicate that when a constant enthalpy throttling line passes the freezing point temperature and approaches the spinodal line, the throttling process can result in sublimation of solid-state CO_2 which may cause a blockage. Therefore, this simulation can be used to explore how changing initial state conditions, CO_2 pressure ranges, and thermomechanical characteristics may result in the blockage of the pressure relief passage and unsafe conditions for users. [DOI: 10.1115/1.4071445]

1 Introduction

Heating and cooling technology in commercial and residential buildings produces carbon emissions in the U.S. that contribute to global warming. One solution is the use of electrically powered heat pumps (HPs) instead of natural-gas-fired traditional heating systems for buildings. Initial variations of the HP utilize hydrocarbon-based working fluids, but carbon dioxide (CO_2) refrigerants can reduce climate change effects due to working fluid loss in HPs [1]. These CO_2 refrigerants can be utilized in smart energy systems that power food refrigeration for supermarkets, ice fields, and vehicle air conditioning [2].

During the throttling and pressure-relief valve processes, CO_2 refrigerants in HP systems can change from a gaseous state to a liquid or solid snow state, which may block downstream flow in pipes [3]. This type of process may occur during leakage caused by a system component failure, or due to activation of the pressure relief system that can occur when the system pressure exceeds the safety limit for the system. Previous work investigates this blockage phenomenon and the effects of the blockages on the heat pump system [4–6]. As CO_2 HP design evolves to include pressure-relief manifold systems in which multiple pipes carry the released flow, understanding the thermophysics of the throttling process is important in order to create designs that mitigate the possibility of blockages. Further, the throttling process can result in metastable states during throttling, so a model framework to predict metastable states is needed to accurately predict conditions that result in production of solid CO_2 during venting of pressure relief valves for their safe design. These considerations are especially important in residential applications where blockages could pose a safety risk.

Dry ice formation also affects carbon dioxide flow within carbon capture utilization and storage practices. Particularly, carbon capture utilization and storage technology requires the transportation of CO_2 long distances in high-pressure pipelines. Recent work created valve schemes to more effectively develop reliable safety relief programs for throttling that increases dry ice formation in the pipeline at inlet operating conditions of 24.9–27.5 °C and 8 MPa [7]. Zhao et al. identify that high temperatures at the inlet of the pipeline system combined with multistage choking can help prevent dry ice formation during throttling and pressure relief with the initial conditions of 8, 9, and 13 MPa and 40 °C [8]. Additionally, the dry ice phenomenon within carbon dioxide can occur in oil recovery practices. Li et al. investigate CO_2 working substance in tertiary oil recovery and find idealized operational inlet pressure and temperature metrics for throttling and venting operations to avoid risk like dry ice within the inlet initial operating conditions of 25–30 MPa and 21.9 °C [9]. While these studies investigate similar dry ice formation due to drastic depressurization that causes temperature and pressure

Summer Heat Transfer Conference (SHTC), July 8–10, 2025. SHTC2025.
[1]Corresponding author.
Contributed by the Heat Transfer Division of ASME for publication in the Journal of Heat and Mass Transfer. Manuscript received December 3, 2025; final manuscript received March 10, 2026; published online April 15, 2026. Assoc. Editor: Nenad Miljkovic.

shifts, often the inlet operating conditions of these systems vary from the ones investigated for HP technology. The range of interest for this study is high-temperature CO_2 heat pumps where the high-pressure side expansion valve has supercritical initial points within 7.37–10 MPa at varying temperatures from 30 to 40 °C.

Multiple thermodynamic metrics can be used to predict the metastable, homogenous nucleation points in the heat exchanger throttling trajectory that lead to dry ice formation. The performance of the working fluid in Rankine cycles can be quantified using a previously developed Redlich–Kwong fluid model [10]. Previous studies locate starting points and determine the output parameter stability in the heat pump with regard to coefficient of performance (COP) and efficiency [11,12]. Other studies use the Wilson limit that combines both nucleation theory and Gyarmathy theory to determine when condensation may occur [13,14]. From those studies the supersaturation ratio metric can be used to describe nucleation growth prediction [15]. As the phenomenon of phase change in heat pump pipes exhibits the same phenomenon that occurs in steam turbine condensation, it is possible to glean metrics from studies conducted for steam turbine condensation [16,17]. Therefore, discoveries in one can impact the other and vice versa in terms of fault detection, prediction, and prevention.

It is possible to train fault detection diagnostic programs to predict sublimation based on thermodynamic phenomena and robust numerical modeling. Fault detection diagnostic programs are often controlled by thermodynamic models and metrices, like the ones described above, or data-driven models. In more complex models, artificial intelligence models can be implemented to make the system maintain a suitable COP [18]. In past papers, small data synthetic sampling has been used as a fault detection method in heating ventilation and air conditioning (HVAC) and heat pump systems [19]. Previous studies use training data and artificial intelligence to detect which type of gradual fault is occurring in a heat pump [20]. These fault detection practices can lead to overall improvements of the heat pump system for better efficiency during emergency pressure relief situations.

Several upgrades can be made to the heat pump to improve the system in nonideal operating conditions. Researchers are expanding the field of air source heat pumps operating in cold climates to address challenges in low maximum COP, heating capacity, and variable year-round reliability [21]. Yang et al. [22] evaluate CO_2 air source heat pump technologies in cold regions utilizing energetic and exergetic analysis. They establish the effects of obtainable component efficiency on system heat capacity and COP. Zheng et al. determine optimal pressure and temperatures to increase the COP of the combined system compared to the original system [23]. They in turn use multifactor coupling to demonstrate operating conditions of temperature of water and ambient temperature, heating capacity, and discharge pressure that are ideal for the system.

Other studies add in new components to heat pump systems to determine the effect on COP of the system in relation to temperature and pressure. Cui et al. [24] develop a control strategy to control a water assisted subcooler in a heat pump and investigate the results on mechanical behavior metrics. The changes in their experimentation on the heat pump demonstrate an increase in COP and heating capacity of the system. Another study analyzes transcritical CO_2 heat pumps combined with an auxiliary CO_2 system and determines optimal pressures and temperatures to increase the COP of the combined system compared to the original system [25]. Liu et al. [26] aim to draw connections of final conditions such as discharge pressure and outlet temperature comparing the overall performance of CO_2 single stage heat pump system to vapor injection pump system. The study determines vapor injection heat pump systems have higher heating capacity in low temperatures than the single stage heat pump.

From these studies, it is evident that when investigating the cold climate region, comparable studies set the ambient temperature in a range of −15 °C to 5 °C and the discharge pressure ranges 8.9 MPa to 10.6 MPa. Figure 1 depicts a typical, ideal heat pump cycle in a cold climate, where the desirable temperature inside is 25 °C and the

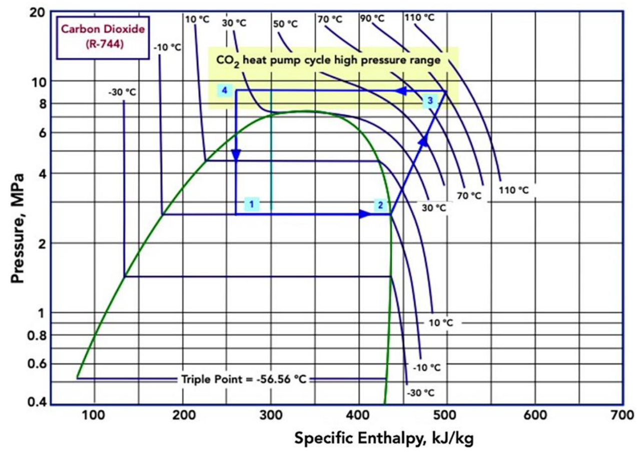

Fig. 1 Mollier diagram with typical heat pump refrigeration cycle (adapted from NIST data and data in the *ASHRAE Handbook of Fundamentals, 2021*)

ambient temperature is 0 °C. The refrigerant temperature drop in the heat exchanger heavily impacts the heat provided to the residential building. If this process is not ideal, there is a possibility for refrigerant leaks from the temperature differential. Similarly, the state points in the highlighted region in Fig. 1 are representative of starting points in the throttling valve and can drastically change the possibility for metastable states to occur.

Given the recent studies of CO_2 heat pumps and their potential use in building HVAC systems, Fig. 1 shows an idealized supercritical CO_2 heat pump cycle that is typical for a building HVAC application that would pump heat from air outside at a design point of −10 °C and deliver it to inside at a design point of 25 °C. This indicates that a throttling process from the high-pressure side of the system resulting from actuating a pressure relief valve or due to a leak would result in throttling from an initial state point roughly in the region between points 3 and 4 on the thermodynamic cycle in Fig. 1 to the surrounding atmospheric pressure conditions. In the study summarized here, we specifically considered throttling process from initial state points, the range indicated in the region between points 3 and 4 on the thermodynamic cycle in Fig. 1, to explore how the initial conditions in this plausible range would affect whether a condensed liquid or solid phase forms during the throttling process. Although this formation is clearly true from indicators in flow features of the leakage pathway or the relief valve system geometry and flow conditions, the objective of this study is to explore how the metastable state thermodynamics can affect the sequence of states encountered during throttling and the probability of a condense phase forming during the process. A model analysis framework was developed in this study that facilitates computation of the changes in state that occur in the CO_2 as its pressure drops in the throttling process, allowing for the possibility that metastable states exist during the process. Predicting the thermophysical properties at each metastable state along the throttling trajectory of this process helps to analyze the nonequilibrium thermodynamics of the system. Completing this analysis can facilitate the better investigation of emerging working fluids in systems like heat pumps, data centers, refrigerants cooling supermarkets, carbon capture and storage, and oil recovery. The details of the model are described in Sec. 2.

2 Materials and Methods

2.1 Statistical Thermodynamic Model. In this study, to predict equilibrium and metastable properties for CO_2, we used the Soave–Redlich–Kwong (SRK) fluid property model [27]. This was chosen because the SRK fluid property model is relatively simple to use for this type of analysis and has been demonstrated to match near saturation properties reasonably well for a wide variety of fluids, including CO_2. A preliminary study using a simpler

Redlich–Kwong fluid model indicated that the SRK model was a better fit to real fluid properties near saturation. Many comparisons for suitable equation of state (EOS) have been developed to determine best practices when investigating CO_2. Log et al. utilize Wagner and Gerg-2008 EOS is also being used to describe CO_2 depressurization [28]. Peng–Robison EOS and experimental data from CO2PipeHaz Project are used to model CO_2 in high-pressure pipelines [29]. Other studies use SRK EOS variants to estimate thermodynamic properties of CO_2 in the supercritical region [30]. Our study chooses to use the modified Soave–Redlich–Kwong model with adjustable constants to analyze CO_2 throttling for its accuracy in modeling simple nonspherical molecular structures in metastable regions. Optimal choice of the fluid property model is not just a matter of the level of agreement with equilibrium saturation properties. A key motivation for our use of the SRK fluid property relation is that it has been shown [31] that SRK property relations can be integrated across the metastable and interspinodal conditions in the interfacial region between liquid and vapor bulk phases to achieve a prediction of fluid surface tension. Since it requires accurate prediction of the metastable state variations to achieve accurate surface tension values by this method, the good agreement of the surface tension predictions with accepted values suggests that the SRK property model can provide an appropriately accurate prediction of the metastable states of interest in this study.

Figures 2(*a*) and 2(*b*) illustrate the fit of SRK model predictions to recommended values of saturation pressure and surface tension for CO_2 tabulated in the ASHRAE Handbook of Fundamentals as a function of temperature [32]. In Fig. 2(*a*), the SRK fluid model was used in capillary theory calculations to predict surface tension at an acentric factor value typical of CO_2 [31]. The good agreement with recommended surface tension values is particularly significant to this study. The capillarity theory calculations to determine surface tension integrate properties across the liquid–vapor interface, which spans the metastable and intrinsically unstable regions for the fluid. The fact that the mean absolute deviation of the model-predicted surface tension values from corresponding accepted values for CO_2 suggests that the SRK model representation of properties in those regimes is appropriate for CO_2. Since in this study we want to predict metastable state properties and the limits of intrinsic stability, this suggests that the SRK model is an appropriate choice for this study. Also, the close agreement between SRK model predictions and recommended vapor pressure data is also a desired feature for our model. Therefore, we selected the SRK fluid property model for this study based on this assessment of its capability to provide a high-fidelity prediction of metastable states that can arise in the throttling process. The objective of this study is to demonstrate the use of an equation of state for assessing regime transitions and focus on ranges of conditions where HP supercritical cycles are likely to occur. The value of the paper is evaluating and analyzing the framework, and over time one can expect increasingly better EOS models to be developed, and those EOS can be implemented into the framework presented in this paper.

Consistent with the earlier model development by, for example, Wemhoff [31], to implement the use of the Soave–Redlich–Kwong fluid property model to predict equilibrium and metastable properties for CO_2, the following form of the partition function relation was adopted:

$$\ln Q = N + \frac{3N}{2}\ln\left(\frac{2\pi M k_B T(V - Nb_{\mathrm{SRK}})^{2/3}}{N^{2/3}h^{2/3}}\right) + N\ln\left(\frac{T}{\sigma_S\theta_r}\right) + \frac{Na_{\mathrm{SRK}}\alpha_{\mathrm{SRK}}}{b_{\mathrm{SRK}}k_BT}\ln\left(\frac{V + Nb_{\mathrm{SRK}}}{V}\right) \quad (1)$$

This equation form was chosen with a suitable choice of the function $\alpha_{\mathrm{SRK}}(T_r)$ standard relations obtained from statistical thermodynamics (see Ref. [33])

$$P = k_BT\left(\frac{\partial \ln Q}{\partial V}\right)_{T,N} \quad (2)$$

$$H = k_BT^2\left(\frac{\partial \ln Q}{\partial T}\right)_{T,N} + PV \quad (3)$$

lead to the Soave–Redlich–Kwong equation of state and an enthalpy relation for a Soave–Redlich–Kwong fluid. So that the equation of state form matches the Soave [27] modification of the Redlich–Kwong equation of state, the relation for α_{srk} is taken to be

$$\alpha_{\mathrm{srk}} = \left[1 + f_{\mathrm{srk}}\left(1 - T_r^{\frac{1}{2}}\right)\right] \quad (4a)$$

$$f_{\mathrm{srk}} = 0.480 + 1.574\omega - 0.176\omega^2 \quad (4b)$$

Since this study specifically focused on CO_2, the value of the acentric factor ω was taken to be 0.239 which is in the recommended range for CO_2 [34]. This results in a value of 0.846 for f_{SRK}.

Using the relations above and the ln$Q$ equation (1) to evaluate the derivatives, relations for the equation of state and enthalpy were derived and converted to dimensionless forms in terms of reduced properties normalized with critical values

$$P_r = P/P_c,\ T_r = T/T_c,\ v_r = \hat{v}/v_c,\ \rho_r = \hat{\rho}/\rho_c \quad (5a)$$

$$h_r = \hat{h}/(N_A k_B T_c) \quad (5b)$$

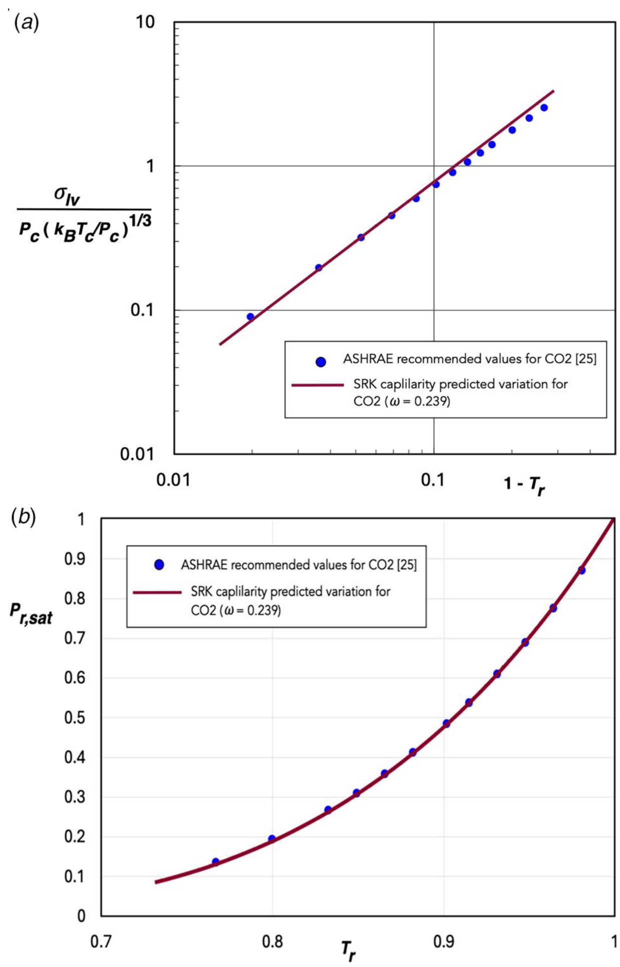

Fig. 2 Comparison of surface tension (*a*) and saturation vapor pressure and (*b*) variations for CO_2 predicted using the Soave–Redlich–Kwong fluid model with corresponding values for CO_2 tabulated in the ASHRAE *Fundamentals* handbook 2021 [25]

Here, the circumflex accent denotes molar properties (e.g., $\hat{v}$ is molar specific volume (m^3/kmol) and $\hat{\rho}$ is molar density (kmol/m^3)). The resulting equations are

$$P_r = \frac{3T_r}{v_r - b_r} - \frac{a_r \alpha_{srk}}{v_r(v_r + b_r)} \tag{6}$$

$$h_r = \left(\frac{5}{2} + \frac{v_r}{v_r - b_r}\right)T_r - 4.93398\left[\ln\left(\frac{v_r + b_r}{v_r}\right)\left(\alpha_{srk} - T_r\frac{d\alpha_{srk}}{dT_r}\right) + \frac{b_r\alpha_{srk}}{v_r + b_r}\right] \tag{7}$$

Here, $\alpha_{srk}(T_r)$ is a function only of reduced temperature T_r, and a_r and b_r are fixed numerical constants: $a_r = 3.84732$, $b_r = 0.25992$ (also noted in Table 1). Since Eq. (7) indicates that $h_r = f(T_r, v_r)$, basic calculus dictates that

$$dh_r = \left(\frac{\partial h_r}{\partial T_r}\right)_{v_r} dT_r + \left(\frac{\partial h_r}{\partial v_r}\right)_{T_r} dv_r \tag{8}$$

and differentiating the h_r equation above yields

$$\left(\frac{\partial h_r}{\partial T_r}\right)_{v_r} = \left(\frac{5}{2} + \frac{v_r}{v_r - b_r}\right) - 4.93398\,\ln\left(\frac{v_r + b_r}{v_r}\right)\frac{d}{dT_r}\left(\alpha_{srk} - T_r\frac{d\alpha_{srk}}{dT_r}\right) + \frac{4.93398}{v_r + b_r}\left(\frac{d\alpha_{srk}}{dT_r}\right) \tag{9}$$

$$\left(\frac{\partial h_r}{\partial v_r}\right)_{T_r} = T_r\left[\frac{1}{v_r - b_r} - \frac{v_r}{(v_r - b_r)^2}\right] - 4.93398\left(\alpha_{srk} - T_r\frac{d\alpha_{srk}}{dT_r}\right) \times \left[\frac{1}{(v_r + b_r)} - \frac{1}{v_r}\right] + \frac{4.93398 b_r \alpha_{srk}}{(v_r + b_r)^2} \tag{10}$$

For constant enthalpy throttling, in Eq. (8), we set $dh_r = 0$ and can use the right size of each of the relations (9) and (10) to evaluate the partial derivatives. The result can be expressed as

$$dT_r = -\left[\frac{\left(\frac{\partial h_r}{\partial v_r}\right)_{T_r}}{\left(\frac{\partial h_r}{\partial T_r}\right)_{v_r}}\right] dv_r \tag{11}$$

Likewise, since Eq. (6) indicates that $P_r = f(v_r, T_r)$, basic calculus dictates that

$$dP_r = \left(\frac{\partial P_r}{\partial v_r}\right)_{T_r} dv_r + \left(\frac{\partial P_r}{\partial T_r}\right)_{v_r} dT_r \tag{12}$$

and differentiating the equation of state yields

$$\left(\frac{\partial P_r}{\partial v_r}\right)_{T_r} = -\frac{3T_r}{(v_r - b_r)^2 + \frac{a_r\alpha_{srk}(2v_r + b_r)}{(v_r^2 + v_r b_r)^2}} \tag{13}$$

$$\left(\frac{\partial P_r}{\partial T_r}\right)_{v_r} = \frac{3}{v_r - b_r} - \frac{a_r d\alpha_{srk}/dT_r}{v_r(v_r + b_r)} \tag{14}$$

Substituting the right side of Eq. (11) into Eq. (12) to eliminate dT_r and rearranging yields

$$\frac{dv_r}{dP_r} = f_1(v_r, T_r) = \frac{1}{\left(\frac{\partial P_r}{\partial v_r}\right)_{T_r} - \left[\frac{(\partial h_r/\partial v_r)_{T_r}}{(\partial h_r/\partial T_r)_{v_r}}\right]\left(\frac{\partial P_r}{\partial T_r}\right)_{v_r}} \tag{15}$$

Combining Eqs. (11) and (15) to obtain

$$(dT_r/dP_r) = (dT_r/dv_r)(dv_r/dP_r)$$

yields

$$\frac{dT_r}{dP_r} = f_2(v_r, T_r) = \frac{-\left[\frac{(\partial h_r/\partial v_r)_{T_r}}{(\partial h_r/\partial T_r)_{v_r}}\right]}{\left(\frac{\partial P_r}{\partial v_r}\right)_{T_r} - \left[\frac{(\partial h_r/\partial v_r)_{T_r}}{(\partial h_r/\partial T_r)_{v_r}}\right]\left(\frac{\partial P_r}{\partial T_r}\right)_{v_r}} \tag{16}$$

Note that Eqs. (15) and (16) form a system of coupled nonlinear ordinary differential equations that can be solved here with boundary conditions of initial values of $v_r = v_{r0}$ and $T_r = T_{r0}$ at an initial reduced pressure P_{r0}. Note that the right sides of Eqs. (15) and (16) are functions of v_r and T_r that are dictated by Eqs. (9), (10), (13), and (14). This system of ordinary differential equations (ODEs) can be solved by a variety of computational schemes. Here, to simulate an adiabatic isenthalpic throttling process, we used a standard fourth-order Runge–Kutta method to compute state variables v_r and T_r as P_r was decreased by successive small steps, simulating the depressurization during the throttling process. At each state determined in this way, we also computed other thermodynamic parameters from the SRK model equations to facilitate whether the state is likely to be in thermodynamic equilibrium or in a metastable state, and how close the state is to the limit of intrinsic stability. For each new T_r value computed in the stepwise depressurization simulation executed using the Runge–Kutta scheme, the equilibrium saturation pressure $P_{r,sat}(T_r)$, the compressibility $(\partial P_r/\partial v_r)_{T_r}$, and the spinodal pressure for reduced temperature T_r were determined from the SRK property model. Determining the thermophysical properties at varying metastable states helped to analyze the nonequilibrium thermodynamics of this process.

For saturated vapor and liquid at equilibrium, the chemical potential of the two phases must be the same. A relation for the chemical potential μ (per molecule) was derived using the thermodynamic relation linking chemical potential to

$$\mu = -k_B T(\partial \ln Q/\partial N)_{V,T} \tag{17}$$

Evaluating the partial derivative by differentiating the ln$Q$ equation and nondimensionalizing yields a relation for the reduced chemical potential μ_r as a function of reduced temperature and reduced specific volume. For a specified temperature, evaluating the right side of the equation first for vapor (v_{rv}) and then for the liquid (v_{rl}) and subtracting them leads to the following relation for the difference in chemical potential between the phases ($\Delta\mu_{rlv}$):

$$\Delta\mu_{rlv} = -T_r\ln\left(\frac{v_{rv} - b_r}{v_{rl} - b_r}\right) + T_r b_{srk}\left(\frac{1}{v_{rv} - b_r} - \frac{1}{v_{rl} - b_r}\right) - \frac{a_r\alpha_{srk}}{3b_r}\ln\left(\frac{v_{rl}(v_{rv} + b_r)}{v_{rv}(v_{rl} + b_r)}\right) - \frac{a_r\alpha_{srk}}{3}\left(\frac{1}{v_{rv} + b_r} - \frac{1}{v_{rl} + b_r}\right) \tag{18}$$

Table 1 Constant variables (ω is specific to CO_2)

Constant	Value
a_r	3.84732
b_r	0.25992
ω	0.239

For the new reduced temperature determined after a step in the Runge–Kutta scheme, the corresponding reduced saturation pressure at that temperature was determined using the following iterative scheme:

(i) The pressure after the most recent integration step was used as a first guess for $P_{r,\mathrm{sat}}$.

(ii) For specified T_r and guessed $P_r = P_{r,\mathrm{sat}}$, the equation of state (Eq. (6)) is a third-order polynomial. Its three roots were determined using a root solver. v_{rl} was set to the smallest root, and v_{rv} was set to the largest root.

(iii) T_r and the computed v_{rl} and v_{rv} from step (ii) were substituted into the right side of Eq. (18). If the right size of Eq. (18) was not sufficiently close to zero, the guessed value of $P_{r,\mathrm{sat}}$ was corrected, and step (ii) was repeated. If the absolute value of the right side of Eq. (18) was sufficiently small ($<10^{-8}$), then the computed value of $P_{r,\mathrm{sat}}$ was taken to be the SRK prediction of $P_{r,\mathrm{sat}}(T_r)$.

The compressibility $(\partial P_r/\partial v_r)_{T_r}$, at the new reduced temperature and reduced specific volume for the throttling process, was computed using Eq. (13), evaluating the right side by substituting the new T_r and v_r computed by the Runge–Kutta scheme for the just-completed integration step.

The spinodal pressure condition at each T_r was determined by finding the root spinodal specific volume value that makes $(\partial P_r/\partial v_r)_{T_r} = 0$ at the local reduced temperature T_r. The left side of Eq. (13) is set to zero, T_r on the right side of this equation is set to the recently determined T_r value, and the resulting right-side relation is solved to find its v_r root that corresponds to the spinodal condition. The spinodal pressure is then computed from the equation of state (Eq. (6)) using the spinodal root solution for v_r and the temperature T_r. As the state changes during depressurization, the proximity to the spinodal condition is indicated by how close $(\partial P_r/\partial v_r)_{T_r}$ is to zero, and how close the pressure at that step is to the computed spinodal pressure.

2.2 Throttling Algorithm. The overall throttling process computation scheme was comprised of the following algorithm steps:

(1) The initial starting values of $v_r = v_{r0}$ and $T_r = T_{r0}$ are set, and the corresponding $P_r = P_{r0}$ is computed from the equation of state (6). The pressure integration step for the Runge–Kutta scheme is set to ΔP_r. The Runge–Kutta scheme used here is the well-known fourth-order scheme described by Jaluria [35]. The pressure step size ΔP_r was varied from -0.01 to -0.001, and our results indicated that the computed state parameter changed by a negligible amount when ΔP_r was reduced from -0.005 to -0.001. We therefore adopted $\Delta P_r = -0.001$ for all our subsequent computations.

(2) For v_r and T_r at the beginning of the pressure step at reduced pressure P_r, the P_r and h_r derivatives, as needed for the Runge–Kutta scheme, were computed using Eqs. (9), (10), (13), and (14), and those results were used to compute dv_r/dP_r and dT_r/dP_r at P_r using Eqs. (15) and (16).

(3) Then, the first derivative relations for dv_r/dP_r and dT_r/dP_r from step (ii) were used in the fourth order Runge–Kutta method to predict v_r and T_r at $P_r + \Delta P_r$.

(4) For the computed value of $(T_r)_{P_r+\Delta P}$ at the next P_r location in the integration, the saturation pressure $P_{r,\mathrm{sat}}(T_r)$ at reduced temperature $(T_r)_{P_r+\Delta P}$ was computed using the iterative scheme with steps (i)–(iii) described in Sec. 2.1.

(5) For the computed values of $(T_r)_{P_r+\Delta P}$ and $(v_r)_{P_r+\Delta P}$ at the next P_r location in the integration, Eq. (13) was solved (using a root solver) to compute $v_{r,\mathrm{spin}}$ for $(T_r)_{P_r+\Delta P}$ that makes $(\partial P_r/\partial v_r)_{T_r} = 0$. Then, when setting $T_r = (T_r)_{P_r+\Delta P}$ and $(v_r = (v_r)_{P_r+\Delta P}$, the equation of state (6) is used to calculate the reduce pressure at the spinodal condition $P_{r,\mathrm{spin}}$.

(6) If the exit pressure $P_{r,\mathrm{exit}}$ has been reached or exceeded, quit the computation. If $P_r < P_{r,\mathrm{exit}}$, loop back to step (2).

This algorithm was implemented in a MATLAB program. A value of -0.001 for ΔP_r was found to produce predictions that did not change significantly if ΔP was reduced further, and the results were concluded to be step size independent. Although we acknowledge that throttling flows can be significantly affected by flow features of the leakage pathway or the relief valve system geometry and flow conditions, the objective of this study is to explore how the metastable state thermodynamics affects the sequence of states encountered during throttling and the probability of a condense phase during the process. Our results and their relevance to these issues are discussed in Sec. 3.

3 Model Prediction Results

3.1 Prediction of Spinodal Limits That May Affect Throttling. To explore the throttling process behavior at typical high-pressure side (for an electronic expansion valve) starting points for CO_2 in a heat pump, we used the throttling model analysis described above to compute the throttling process behavior for supercritical state points like the six example points indicated by orange circular symbols in Fig. 3. For the CO_2 HP, the pressure from the heat pump compressor needs to be high enough so the supercritical heat rejection process refrigerant temperature is above ambient temperature for the room (25 °C); the ideal working fluid temperature for this heat rejection process would then be 30 °C or above to drive the heat flow into the room. Additionally, the evaporator temperature should be at -10 °C to help to demonstrate pulling heat out of the air in cold climates. Based on the thermodynamic cycle demonstrated from these requirements, a suitable range to pull the six points from are around the 30 °C to 36 °C point, at reduced temperatures $T_r = (0.98, 1.01, 1.04, 1.045, 1.06, 1.19)$ for the supercritical pressure of $P = 9$ MPa ($P_r = 1.22$). Conditions for these starting points are indicated in Fig. 3 and Table 2. For adiabatic throttling, the process line should be vertical on the Mollier diagram, and the vertical lines for some of the starting points indicate the path of the process on this diagram. For the left-most four supercritical starting points, we found that as the pressure in throttling fluid dropped, it eventually reached a point where throttling fluid pressure matches the spinodal pressure for the system temperature. This implies that that state point is on the spinodal curve. As illustrated in Fig. 3, for some starting points to the right of the critical point, the constant enthalpy line crossed the spinodal curve twice. And, as expected, for initial state points like point 7 that is far to the right of the critical point, throttling results in states with progressively lower pressure that are all in the superheated vapor range.

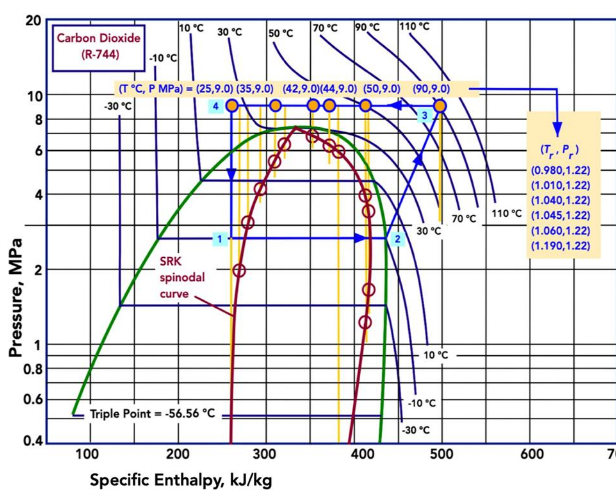

Fig. 3 Throttling from select initial supercritical states and determination of points on the SRK spinodal curve

Table 2 Initial state reduced properties at $P_r = 1.22$

	T_r	v_r
Point 1	0.98	0.5683
Point 2	1.01	0.6927
Point 3	1.04	1.1230
Point 4	1.045	1.2020
Point 5	1.06	1.3880
Point 6	1.190	2.2350

By running throttling calculations for multiple starting points, we were able to establish the curve consisting of the locus of points in the two spinodal curves that converge to the critical point. The resulting predictions of the spinodal curves on the Mollier diagram for CO_2 are shown in Fig. 4.

3.2 Wilson Line Conditions. The Wilson line defines the onset of liquid condensation in a throttled vapor flow as a consequence of density-fluctuation-driven nucleation in a metastable supersaturated vapor flow [36,37]. In a very recent study, Petruccelli et al. [38] plotted experimental data obtained by Bier et al. [12] for the Wilson line conditions in a throttled CO_2 flow in terms of reduced pressure and temperature. The Bier CO_2 data are plotted in this form in Fig. 5. Plotted in this form, the data are consistent with the idealization that the measured Wilson line pressures for CO_2 are close to halfway between the saturation line and the spinodal. Based on this idealization, the Wilson line for CO_2 was added to the Mollier diagram to obtain the version shown in Fig. 6. Note that the addition of the Wilson line reflects the fact that the strongly increasing density fluctuations predicted to occur as the state gets closer to the spinodal line increase the probability that nucleation of an embryonic phase will initiate transition from a metastable fluid to a combination of saturated liquid and vapor phases.

3.3 Starting Point Regimes That Give Rise to Different Condensed Phase Nucleation Behavior. Figure 6 provides a framework for predicting how throttling supercritical CO_2 will react to decreasing pressure in the throttling process for starting points near $P_r = 1.22$ in the supercritical region. To the left of the critical point, for $0.98 < T_r < 1.02$, throttling depressurizes supercritical fluid, which causes a shift to a superheated liquid that becomes increasingly superheated as the pressure drops. As it gets close to the spinodal curve, nucleation of bubbles is expected to be initiated, transforming it to a mixture of saturated liquid and vapor. If the fluid depressurizes to atmospheric pressure, its temperature will drop below the triple point temperature, and solidification is likely.

For starting points near $P_r = 1.22$ and $1.02 \le T_r < 1.05$, depressurizing supercritical fluid will cause the state point to shift vertically down along a constant enthalpy line, causing it to enter the region between the spinodal curves which lacks intrinsic stability. In doing so, density fluctuations are expected to cause it to almost immediately transition to a mixture of saturated liquid and vapor. Again, if the fluid continues to depressurize to atmospheric pressure, its temperature will drop below the triple point temperature, and some solidification is likely.

For starting points near $P_r = 1.22$ and $1.05 \le T_r < 1.08$, depressurizing supercritical fluid will move the state point down into the metastable supersaturated vapor region. If it penetrates to the left of the Wilson lime limit, larger density fluctuations near the spinodal line may drive nucleation to initiate formations of liquid droplets. If the throttling pressure variation stays to the right of the Wilson curve, density fluctuations may be small enough to avoid formation of liquid droplets via nucleation.

On the far right of the heat rejection process for the heat pump cycle, at starting points near $P_r = 1.22$ and $1.08 \le T_r < 1.19$, depressurizing supercritical fluid will move the state point down a constant enthalpy line that is entirely to the right of the saturated vapor line. As a result, supercritical fluid is depressurized to a single-phase, lower density gas.

3.4 Predicted Throttling Pressure Variations for Example Starting Points. As noted above, the rightmost example starting point in Fig. 4 ($(T_r, P_r) = (1.19, 1.22)$), a constant enthalpy throttling process will simply depressurize the supercritical fluid

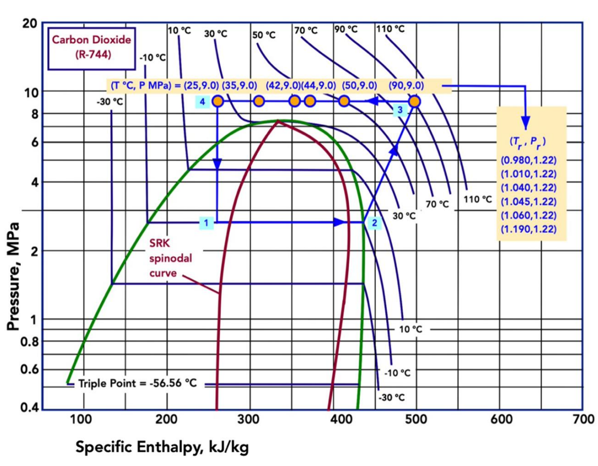

Fig. 4 CO_2 spinode curves predicted by SRK model analysis of throttling from multiple initial supercritical states

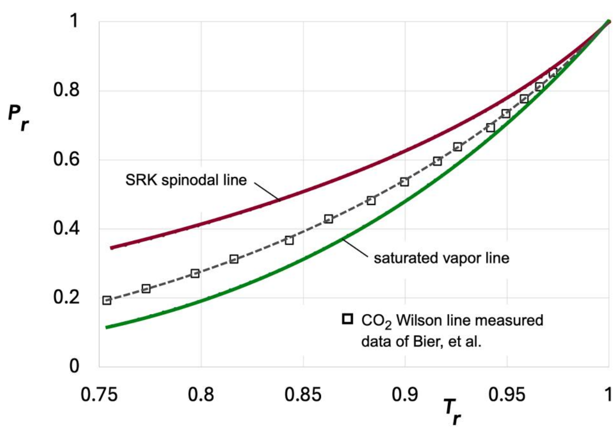

Fig. 5 CO_2 Wilson line measured data of Bier et al. [12] plotted in terms of reduced temperature and pressure

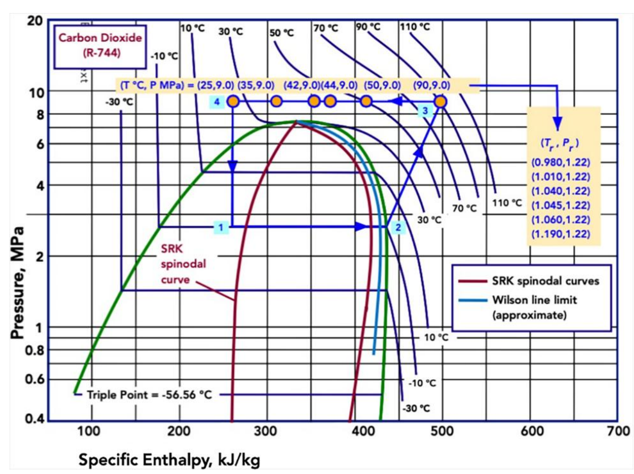

Fig. 6 CO_2 spinode curves predicted by model analysis of throttling from multiple initial supercritical states and the Wilson line limit for CO_2

to a superheated gas, without getting near the saturated vapor line. Starting points in this range are therefore predicted to not result in nucleation and growth of a condensed (liquid or solid) phase as it depressurizes. However, for the other example starting points, the model analysis predicts that the formation of a condensed phase during the constant enthalpy depressurization is likely, but it depends on the proximity of the throttling-process state points to the spinodal curves.

Figures 7 and 8 show the predicted variation of the CO_2 reduced pressure as the throttling process proceeds. Temperature steadily drops as the pressure is lowered, so it is taken as a metric of progress in the throttling process, and the predicted throttled fluid reduced pressure and the reduced saturation pressure and spinodal pressure are plotted at each temperature level as throttling proceeds. Since the temperature axis increases to the right, the throttling process trajectory is traced from right to left on the graph which is indicated by the red arrow.

Figure 7 shows isenthalpic throttling from a starting point in the supercritical range just to the left of the critical point in Fig. 4. The line that is labeled initial state in Fig. 7 indicates the sequence of states predicted by the model for the throttling process from the starting point in the upper right to subsequent points moving downward and to the left. As expected, Fig. 7 indicates the fluid pressure dropping, which brings the state in the metastable superheated liquid region between the saturation curve and the spinodal curve. The metastable superheated liquid may nucleate a vapor phase if the state point comes close enough to the spinodal point.

The Wilson line mentioned earlier is a transition to onset of nucleation of a condensed phase observed for throttling starting in the supercritical region to the right of the critical point. For such circumstances, supercritical fluid becomes a supersaturated vapor which may nucleate a liquid CO_2 phase if it comes close enough to the spinodal curve (becomes highly supersaturated). An example of the model prediction of the process line for isenthalpic throttling in circumstances of this sort is shown in Fig. 8. It is noteworthy that Fig. 7 is an example of throttling that converts a supercritical fluid to a dense metastable liquid that becomes less stable as the spinodal is approached. Statistical thermodynamic analysis indicates that the level of heterophase density fluctuations will sharply increase as the spinodal condition is approached [33], and these can give rise to density fluctuations that may initiate nucleation of a low-density vapor phase in the metastable liquid. Consistent with the Wilson line analysis in this regime, we do expect that onset of a vapor phase nucleation will occur when a state point is near the middle of the region between the saturation curve and the spinodal. However, this is not the type of system transition for which the Wilson transition analysis is typically assumed to apply, and so a Wilson limit line is not shown for this case. The Wilson limit is typically associated with conditions more like those considered in Fig. 8. The starting point in that case is in the supercritical region to the right of the critical point. In such cases, the throttling supercritical fluid transitions to metastable supersaturated vapor, which may give rise to nucleated droplets or solid phase particulates if it approaches states close to the spinodal curve and density fluctuations become extreme. Because the Wilson limit modeling and measurement are relevant to this type of supersaturated vapor transition, we include a prediction of the Wilson limit in Fig. 8 based on a fit to data obtained for CO_2.

In Fig. 8, the system pressure enters the subcritical region for $T_r < 1.0$ and follows a path close to, but just below, the spinodal curve. This implies the metastable fluid system states do not reach the limit of intrinsic stability, but they are substantially beyond the Wilson line limit of stability, implying that nucleation will lead to a transition to a liquid–vapor two phase system. Note in Fig. 8 that once the system process line intersects the spinodal, we terminate further computation of the process line because the system will lack intrinsic stability once it reaches a state on the spinodal curve, and the validity of the analysis equations used here becomes uncertain beyond that point.

3.5 Prediction of State Variations for Throttling With Heat Input or Cooling.

In Sec. 2.1, in the derivation of the differential equations (15) and (16) describing the property changes during

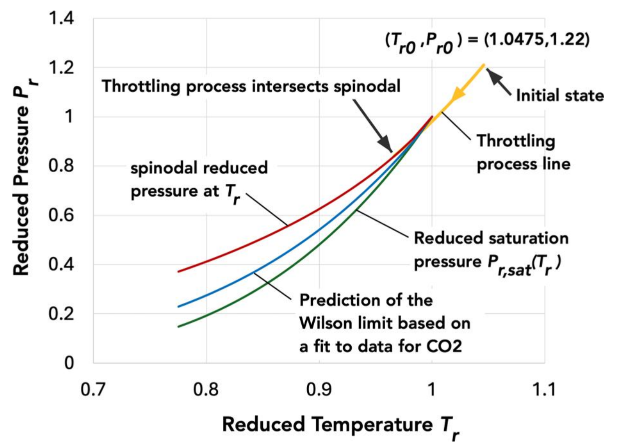

Fig. 8 Pressure trajectory analysis for isenthalpic throttling of CO_2 with (T_r, P_r)=(1.0475, 1.22). Also shown is the prediction of the Wilson limit based on a reduced property fit to data for CO_2.

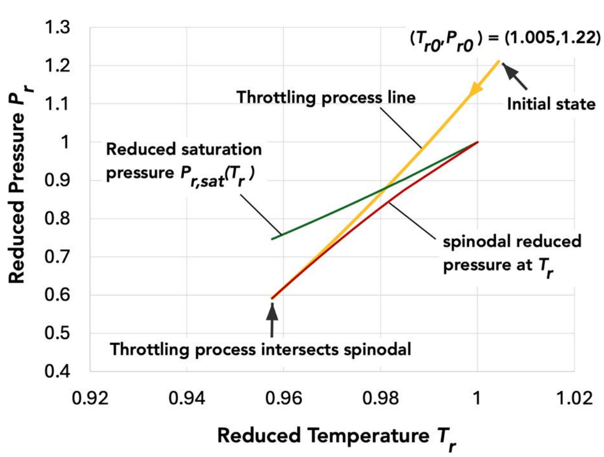

Fig. 7 Pressure trajectory analysis for isenthalpic throttling of CO_2 with (T_{r0}, P_{r0})=(1.005, 1.22)

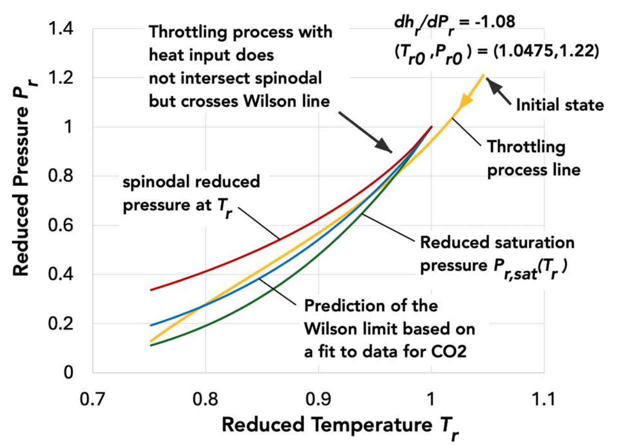

Fig. 9 Wilson limit and pressure trajectory analysis for throttling with heat input $dh_r/dP_r = -1.08$. Otherwise, the starting point and throttling process are the same as those modeled in Fig. 8 (for starting point (T_r, P_r)=(1.0475, 1.22)).

throttling, the differential change in reduced enthalpy was set to zero to model a constant enthalpy throttling process. Real relief valve processes may be close to isenthalpic, or there may be significant heat input or cooling of the flow during the process. The analysis framework developed in this study can, in fact, be easily modified to a form that can analyze throttling processes with heat input or removal. Retaining the dh_r term in Eq. (8) leads to the following alternate forms of Eqs. (15) and (16):

$$\frac{dv_r}{dP_r} = f_1(v_r, T_r) = \frac{\left[1 - \frac{\left(\frac{\partial P_r}{\partial T_r}\right)_{v_r} \frac{dh_r}{dP_r}}{\left(\frac{\partial h_r}{\partial T_r}\right)_{v_r}}\right]}{\left[\left(\frac{\partial P_r}{\partial v_r}\right)_{T_r} - \left(\frac{\partial P_r}{\partial T_r}\right)_{v_r}\left(\frac{\partial h_r}{\partial v_r}\right)_{T_r} \Big/ \left(\frac{\partial h_r}{\partial T_r}\right)_{v_r}\right]} \tag{19}$$

$$\frac{dT_r}{dP_r} = f_2(v_r, T_r) = \left[\left[\frac{\frac{dh_r}{dP_r}}{\left(\frac{\partial h_r}{\partial T_r}\right)_{v_r}}\right] - \left[\frac{\left(\frac{\partial h_r}{\partial v_r}\right)_{T_r}}{\left(\frac{\partial h_r}{\partial T_r}\right)_{v_r}}\right] \times \frac{\left[1 - \frac{\left(\frac{\partial P_r}{\partial T_r}\right)_{v_r} \frac{dh_r}{dP_{r_r}}}{\left(\frac{\partial h_r}{\partial T_r}\right)_{v_r}}\right]}{\left[\left(\frac{\partial P_r}{\partial v_r}\right)_{T_r} - \left(\frac{\partial P_r}{\partial T_r}\right)_{v_r}\left(\frac{\partial h_r}{\partial v_r}\right)_{T_r} \Big/ \left(\frac{\partial h_r}{\partial T_r}\right)_{v_r}\right]}\right] \tag{20}$$

Equations (19) and (20) contain the parameter dh_r/dP_r. In a throttling flow through some kind of passage or orifice, over a flow length dz, friction will result in a pressure gradient dP_r/dz, and dh_r/dz over that flow length will be associated with the heat transfer rate to the flow per unit length q' divided by mass flow rate and specific heat at constant pressure. Hence, dh_r/dP_r is a parameter that specifies the ratio dP_r/dz, and $dh_r/dz = q'/\dot{m}c_p$

$$dh_r/dP_r = \frac{dh_r/dz}{dP_r/dz} = \frac{q'/\dot{m}c_p}{dP_r/dz}$$

Note that setting dh_r/dP_r to zero reduces Eqs. (19) and (20) to Eqs. (15) and (16) used for constant enthalpy throttling. If a value for dh_r/dP_r is specified, the throttling algorithm indicated above can be used to predict state changes for throttling with heat addition or cooling. Because throttling always lowers pressure (a negative change), it follows that

$$\text{heating} \rightarrow \text{increasing } h_r \rightarrow \frac{dh_r}{dP_r} < 0$$

$$\text{cooling} \rightarrow \text{decreasing } h_r \rightarrow \frac{dh_r}{dP_r} > 0$$

To explore the impact of heating, the throttling algorithm computation was repeated for conditions identical to those considered for the process analyzed in Fig. 8 except that heating was added corresponding to $dh_r/dP_r = -1.08$. The resulting throttling process curve is shown in Fig. 9. Comparing Figs. 8 and 9 indicates that the heat input has the effect of moving the throttling process line downward, in a way that reduces the likelihood that the states encountered in the process will cross the spinodal line. For the heating level specified, the heated throttling process line for the starting point in Fig. 9 enters the metastable range and crosses the Wilson line but does not cross the spinodal line. The trend suggests that if the heat rate were increased, the downward shift of the process line may result in the process not crossing the Wilson line, which could prevent a condensate phase from nucleating. The trends also suggest that if the throttling fluid is cooled, the process line would shift upward, making it more likely to cross the spinodal line, which would increase the probability that the throttling supercritical fluid would become unstable and bifurcate into a two-phase liquid and vapor mixture. The insight into how heating or cooling may affect throttling processes clearly can be valuable for understanding how throttling of supercritical CO_2 can be altered by heat input or cooling during the process.

4 Conclusion

Although somewhat idealized, the SRK statistical-thermodynamics-based model analysis of CO_2 throttling provides a means to predict how nonequilibrium thermodynamics affect CO_2 refrigerant metastable state properties (enthalpy, temperature, and volume) exhibited during throttling through a leakage path or pressure relief valve in heat pump technologies. This provides a capability to understand and predict the nature of phase change processes that may occur in this type of throttling process, and how high-pressure side initial state conditions can affect the state of discharged CO_2 released into the surroundings. Our results indicate that the SRK fluid model is useful for this type of analysis of CO_2 because its property predictions near saturation conditions compare favorably to corresponding ASHRAE published data and throttling calculations with it are relatively simple to implement. We have demonstrated that this analysis framework can be used for isenthalpic throttle expected for adiabatic flows, and it can be adapted to include effects of heat input or cooling of the flow. While we specifically used the Soave–Redlich–Kwong fluid property model for this study because its near saturation property predictions for CO_2 agree well with recommended values, other fluid models such as the Peng–Robinson or Span–Wagner model could be used in the throttle algorithm described here. This framework could also be useful as a property subroutine for computational fluid dynamics type modeling of throttling processes. And it is noteworthy that this modeling framework can be applied with reasonable accuracy to a wide variety of working fluids other than CO_2, with model constants adjusted appropriately for the fluid type.

By combining the understanding of the nonequilibrium thermodynamics of CO_2 during throttling provided by this type of model with fluid dynamics and heat transfer, one can predict high-pressure side state conditions (for an electronic expansion valve) that are more likely to result in ice formations on the macro and microscales. The results of this type of model prediction can contribute to the design of next generation CO_2 heat pump systems for different applications like heating and cooling residential buildings or carbon capture and storage by providing a means of predicting the potential for solid CO_2 snow formation during accidental leakage or pressure relief valve operation. The prediction of the throttling model described here can also help guide experimental studies of throttling that aim to simulate CO_2 leakage or pressure relief valve function.

Acknowledgment

Support for this research by the International Institute of Ammonia Refrigeration is gratefully acknowledged. Partial funding for this research was also provided by Chancellor's Fellowship support, the endowment of the A. Richard Newton Chair in Engineering at UC Berkeley, and the National Consortium for Graduate Degrees for Minorities in Engineering (GEM).

Funding Data

- International Institute of All-natural Refrigeration (IIAR) and Natural Refrigeration Foundation (NRF) (CO2 Icing, Award No. 058888).

- University of California Chancellor's Fellowship.
- National Consortium for Graduate Degrees for Minorities in Engineering (GEM).

Data Availability Statement

The datasets generated and supporting the findings of this article are obtainable from the corresponding author upon reasonable request.

Nomenclature

a_r = nondimensionalized constant
b_r = nondimensionalized constant
c_p = specific heat at constant pressure
f_{srk} = SRK model parameter
h = molar specific enthalpy (kJ/kg)
$\dot{m}$ = mass flow rate
N = number of molecules in the system
NA = Avogadro's number
P = pressure
P_{atm} = atmospheric pressure (MPa)
P_r = reduced pressure
P_{rWL} = reduced Wilson's limit pressure
Q = partition function
q' = heat transfer per unit length
T = absolute temperature
T_r = reduced temperature
V = system volume
v_r = reduced volume
γ = gamma constant
θ_r = molecule rotational temperature
μ = chemical potential
σ_s = molecule symmetry number
ω = acentric factor

Subscripts

c = critical point constant
l = liquid
r = reduced property normalized with critical point value
v = vapor

References

[1] Aguilera, J., Meesenburg, W., Ommen, T., Markussen, W., Poulsen, J., Zuhlsdorf, B., and Elmegaard, B., 2022, "A Review of Common Faults in Large-Scale Heat Pumps," Renewable Sustainable Energy Rev., **168**, p. 112826.
[2] Yang, D., Li, Y., Xie, J., and Wang, J., 2022, "Research and Application Progress of Transcritical CO_2 Refrigeration Cycle System: A Review," Int. J. Low-Carbon Technol., **17**, pp. 245–256.
[3] Yamaguchi, H., Biu, X., Sekimoto, K., and Neksa, P., 2010, "Investigation of Dry Ice Blockage in an Ultra-Low Temperature Cascade Refrigeration System Using CO_2 as a Working Fluid," Int. J. Refrig., **34**, pp. 466–475.
[4] Maher, D., Valencia, J., Denton, R., and Bevilacqua, T., 2015, "Strategies for Relieving CO_2 Build-Up in Pipeline Systems," Proceedings of the Mary Kay O'Conner Process Safety Center 18th Annual International Symposium, College Station, TX, Oct. 27–29, Texas A&M University, p. 193711.
[5] Qiao, M., Jing, Z., Zhou, R., Chen, C., Xupeng, Z., Li, Y., and Zou, Q., 2024, "The Throttling Characteristics of Supercritical Carbon Dioxide in the Flowback Process of CO_2 Fracturing," Gas Sci. Eng., **121**, p. 205184.
[6] Pelella, F., Viscito, L., and Mauro, A., 2022, "Combined Effects of Refrigerant Leakages and Fouling on Air-Source Heat Pump Performances in Cooling Mode," Appl. Therm. Eng., **204**, p. 117965.
[7] Qiao, F., Liu, Z., Chen, L., Yu, S., Hu, Y., Yan, X., and Yu, J., 2025, "Experimental Study on the Safety of Dry Ice Freeze Plugging by Throttling Effect During Pressure Relief of Industrial CO_2 Pipeline," Process Saf. Environ. Prot., **197**, p. 107001.
[8] Zhao, Q., Li, Y., and Li, S., 2014, "Safety Control on the Chocking Process of Supercritical Carbon Dioxide Pipeline," Adv. Mech. Eng., **6**, p. 253413.
[9] Li, M., Shen, H., Wang, Y., Ren, J., and Bi, M., 2026, "Experimental Study on Throttling Release of High-Pressure Carbon Dioxide," Appl. Therm. Eng., **285**, p. 129302.
[10] Sunter, D., and Carey, V. P., 2010, "A Thermodynamic Similarity Framework for Assessment of Working Fluids for Solar Rankine Power Generation," ASME J. Sol. Energy Eng., **132**(4), p. 041005.
[11] Wang, D., Li, Y., Guo, Y., Zhu, J., Wang, G., Wang, Y., and Liu, C., 2024, "Experimental Study and Optimization Analysis of Start Control Strategy for the Transcritical Carbon Dioxide Heat Pump," Appl. Therm. Eng., **257**, p. 124344.
[12] Bier, K., Ehrler, F., and Niekrawietz, M., 1990, "Experimental Investigation and Computer Analysis of Spontaneous Condensation in Stationary Nozzle Flow of CO_2-Air Mixtures," *Adiabatic Waves in Liquid-Vapor Systems*, International Union of Theoretical and Applied Mechanics, Springer, Berlin, Heidelberg, pp. 113–127.
[13] Dingilian, K. K., Halonen, R., Tikkanen, V., Reischl, B., Vehkamäki, H., and Wyslouzil, B. E., 2020, "Homogeneous Nucleation of Carbon Dioxide in Supersonic Nozzles I: Experiments and Classical Theories," Phys. Chem. Chem. Phys., **22**(34), pp. 19282–19298.
[14] Ding, H., Wang, C., and Zhao, Y., 2014, "An Analytical Method for Wilson Point in Nozzle Flow With Homogeneous Nucleating," Int. J. Heat Mass Transfer, **73**, pp. 586–594.
[15] Nezebeda, I., and Moucka, F., 2019, "Thermodynamics of Supersaturated Steam: Towards an Equation of State," Fluid Phase Equilib., **484**, pp. 114–121.
[16] Hu, P., Zhao, P., Li, Q., Hou, T., Wang, S., Cao, L., and Wang, Y., 2023, "Performance of Non-Equilibrium Condensation Flow in Wet Steam Zone of Steam Turbine Based on Modified Model," Energy, **267**, p. 126571.
[17] Li, C., Zhang, C., Li, Z., and Jia, W., 2022, "Numerical Study on the Condensation Characteristics of Natural Gas in the Throttle Valve," J. Nat. Gas Sci. Eng., **104**, p. 104689.
[18] Guo, Y., Wang, Y., Liu, Y., Du, C., and Li, Y., 2025, "Optimizing Discharge Pressure Control in Carbon Dioxide Heat Pumps Using Particle Swarm Optimization," Appl. Therm. Eng., **260**, p. 125008.
[19] Zhang, J., Xu, Y., Chen, H., and Xing, L., 2023, "A Novel Building Heat Pump System Semi-Supervised Fault Detection and Diagnosis Method Under Small and Imbalanced Data," Eng. Appl. Artif. Intell., **123**, p. 106316.
[20] Sun, Z., Jin, H., Gu, J., Huang, Y., Wang, X., and Shen, X., 2019, "Gradual Fault Early Stage Diagnosis for Air Source Heat Pump System Using Deep Learning Techniques," Int. J. Refrig., **107**, pp. 63–72.
[21] Zhang, L., Jiang, Y., Dong, J., and Yao, Y., 2018, "Advances in Vapor Compression Air Source Heat Pump System in Cold Regions: A Review," Renewable Sustainable Energy Rev., **81**, pp. 353–365.
[22] Yang, Y., Peng, X., Wang, G., Liu, X., and Wang, D., 2023, "Energetic and Exergetic Analysis of a Transcritical CO_2 Air-Source Heat Pump Water Heating System in the Cold Region," Energy Build., **298**, p. 113558.
[23] Zheng, Z., Song, Y., Wang, S., Yang, X., Cao, F., and Yang, T., 2024, "Multi-Factor Coupling Optimization of Heat Recovery Effectiveness in a Transcritical CO_2 Heat Pump," Int. J. Refrig., **167**, pp. 201–213.
[24] Cui, Q., Dianhang, W., Gao, E., Zhang, K., and Zhang, X., 2023, "Experimental Study on the Performance and Control Strategy of a Water-Cooled Subcooler-Assisted Carbon Dioxide Heat Pump for Combined Cooling and Heating," Energy Convers. Manage., **279**, p. 116761.
[25] Cao, F., Cui, C., Wei, X., Yin, X., Li, M., and Wang, X., 2019, "The Experimental Investigation on a Novel Transcritical CO_2 Heat Pump Combined System for Space Heating," Int. J. Refrig., **106**, pp. 539–548.
[26] Liu, X., Wang, D., Peng, X., Wang, G., and Yang, Y., 2024, "Experimental Study on Performance and Compressor Characteristics of Transcritical CO_2 Heat Pump System," Appl. Therm. Eng., **250**, p. 123524.
[27] Soave, G., 1972, "Equilibrium Constants From a Modified Redlich-Kwong Equation of State," Chem. Eng. Sci., **27**(6), pp. 1197–1203.
[28] Log, A. M., Hammer, M., Deng, H., Austegard, A., Hafner, A., and Munkejord, S., 2024, "Depressurization of CO_2 in a Pipe: Effect of Initial State on Non-Equilibrium Two-Phase Flow," Int. J. Multiphase Flow, **170**, p. 104624.
[29] Martynov, S., Brown, S., Mahgerefteh, H., Sundara, V., Chen, S., and Zhang, Y., 2014, "Modelling Three-Phase Releases of Carbon Dioxide From High-Pressure Pipelines," Process Saf. Environ. Prot., **92**(1), pp. 36–46.
[30] Dong, A., Chen, Y., Zhan, T., Hou, K., He, M., and Zhang, Y., 2025, "Optimization of Crossover SRK Equation of State for Thermodynamic Properties Calculation of CO_2," Fluid Phase Equilib., **587**, p. 114200.
[31] Wemhoff, A. P., 2010, "Extension of the Neoclassical Theory of Capillarity to Advanced Cubic Equations of State," Int. J. Thermophys., **31**(2), pp. 253–275.
[32] ASHRAE, 2021, *ASHRAE Handbook of Fundamentals*, ASHRAE, Peachtree Corners, GA.
[33] Carey, V., 1999, *Statistical Thermodynamics and Microscale Thermophysics*, Cambridge University Press, Cambridge, UK.
[34] Reid, R. C., Prausnitz, J. M., and Poling, B. E., 1987, *The Properties of Gases and Liquids*, 4th ed., McGraw-Hill, New York.
[35] Jaluria, Y., 1996, *Computer Methods for Engineering*, Taylor and Francis, New York, Sec. 8.4.
[36] Wilson, C. T. R., 1897, "Condensation of Water Vapor in the Presence of Dust-Free Air and Other Gases," Philos. Trans. A, **189**, pp. 265–307.
[37] Dobbins, R. A., 1983, "A Theory of the Wilson Line for Steam at Low Pressures," ASME J. Fluids Eng., **105**(4), pp. 414–422.
[38] Petruccelli, G., Grönman, A., and Turunen-Saaresti, T., 2024, "A Novel Numerical Approach for Simulating Low-Pressure and High-Pressure Non-Equilibrium Condensation in Real Gases," Int. J. Multiphase Flow, **171**, p. 104700.